



Understanding the role of the anode on the polarization losses in high-temperature polymer electrolyte membrane fuel cells using the distribution of relaxation times analysis

N. Bevilacqua^a, M.A. Schmid^a, R. Zeis^{a,b,*}

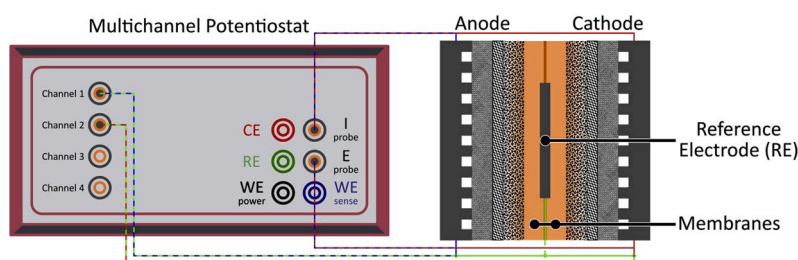
^a Karlsruhe Institute of Technology (KIT), Helmholtz Institute Ulm (HIU), Helmholtzstraße 11, 89081, Ulm, Germany

^b Karlsruhe Institute of Technology (KIT), Institute for Physical Chemistry, Fritz-Haber-Weg 2, 76131, Karlsruhe, Germany

HIGHLIGHTS

- DRT impedance study of a high-temperature PEM fuel cell.
- Understanding the impact of humidification and gas impurities on the fuel cell.
- Developing a suitable reference cell setup for PEM fuel cells.
- Quantifying anode and cathode polarization contributions.

GRAPHICAL ABSTRACT



ARTICLE INFO

Keywords:

High-temperature polymer electrolyte membrane fuel cell (HT-PEMFC)
Distribution of relaxation times analysis (DRT)
Electrochemical impedance spectroscopy (EIS)
Carbon monoxide (CO)
Reference electrode

ABSTRACT

To investigate the role of the anode on the polarization losses of a High-Temperature Polymer Electrolyte Membrane Fuel Cell (HT-PEMFC), we analyzed impedance data using the Distribution of Relaxation Times (DRT) method. Thereby, we varied the operating conditions of the anode (humidification, nitrogen dilution, and carbon monoxide (CO) impurities) to study its impact on Nyquist plot and DRT spectrum. Humidification of the hydrogen was found to dilute phosphoric acid, which is visible in the DRT. Nitrogen dilution of the anode gas slightly increases the Mass Transport (MT) resistance. Furthermore, CO was added to anode gas fed and it impacts the impedance throughout the whole frequency range, specifically the medium and low-frequency range, typically assigned to ORR kinetics and oxygen MT. For a more detailed analysis of the impedance data, a reference electrode was employed to separate the overpotential caused by each electrode. The DRT spectrum of the anode exhibits only one peak at 1 kHz. In the presence of CO, a second peak arises corresponding to side-reactions occurring as the anodic half-cell potential increases. It was found that the cathode is affected by CO on the anode merely by the lowered cell potential and not by CO directly.

1. Introduction

Due to the growing interest of zero-emission technology, the

research in High-Temperature Polymer Electrolyte Membrane Fuel Cells (HT-PEMFCs) has increased over the last decade [1]. They typically operate at temperatures between 140 °C and 200 °C, which presents

* Corresponding author. Karlsruhe Institute of Technology (KIT), Helmholtz Institute Ulm (HIU), Helmholtzstraße 11, 89081, Ulm, Germany.

E-mail address: roswitha.zeis@kit.edu (R. Zeis).

<https://doi.org/10.1016/j.jpowsour.2020.228469>

Received 6 April 2020; Received in revised form 18 May 2020; Accepted 3 June 2020

Available online 28 June 2020

0378-7753/© 2020 The Author(s).

Published by Elsevier B.V. This is an open access article under the CC BY-NC-ND license

(<http://creativecommons.org/licenses/by-nc-nd/4.0/>).

various benefits compared to temperatures between 60 °C and 90 °C, at which Low-Temperature PEMFCs (LT-PEMFCs) are operated [2–5]. A polybenzimidazole (PBI) membrane doped with phosphoric acid is employed to ensure proton conductivity to the reactive sites inside the catalyst layer, as it remains in a liquid state at these high temperatures [6,7]. Operating above the boiling point of water facilitates the water management, as the product water evaporates and is transported out of the cell via the gas phase. Further, the PBI membrane does not need reactant gas humidification due to the proton conductivity provided by phosphoric acid. Thus, the water balance of HT-PEMFCs is simple compared to LT-PEMFCs and the overall power system is more straightforward [8–12]. Also, the operation at higher temperatures improves electrode kinetics, reactant diffusivity, and improves the tolerance toward impurities in the gas stream [2,3,7]. The Carbon Monoxide (CO) tolerance increases from a few parts per million for the LT-PEMFC [13] to up to 5% CO volume in the anode gas stream in case of the HT-PEMFC, which is above conventional steam reformat CO contamination levels [14]. Zhang et al. [15], Das et al. [16], and Araya et al. [17] showed experimentally that the CO poisoning of the catalyst particles is temperature-dependent. Oh et al. [18] validated these findings with numerical simulations. Seel et al. [19] describe the anode overpotential at different temperatures with varying amounts of CO in the anode gas stream and show that the difference of the overpotential between 1% CO and 3% CO at OCV decreases from 100 mV at 140 °C to just 10 mV at 160 °C. An optimum operating temperature concerning cell degradation and CO tolerance lies between 160 °C and 180 °C [15]. The higher operating temperature also improves the utilization of the waste heat in combined heat and power units for stationary applications or fuel processing [20–22]. These advantages allow the HT-PEMFC to be deployed off-grid in remote locations where hydrogen can be produced locally by steam reforming [23–26]. Some reforming processes generate nitrogen as a by-product, which dilutes the hydrogen gas stream. Autothermal natural gas and methanol reformation generate output gases with up to 40% nitrogen. Steam reforming processes contain about 1% nitrogen, but up to 30% CO₂. Both nitrogen and carbon dioxide dilute the anode gas stream when a HT-PEMFC is operated with reformat gases and thus, the impact on the performance is critical to understand [27]. The effect of the presence of nitrogen in the anode gas stream has been previously explored by Waller et al. [6] and the presence of CO₂ dilution has been investigated in great detail by Andreasen et al. [28]. A decrease in the performance of the HT-PEMFC is expected when the anode gas stream is diluted by N₂, which can be attributed to the decrease in the partial pressure of H₂ [29,30]. Due to their similarity in nature, the HT-PEMFC shares many attributes with a phosphoric acid fuel cell (PAFC), such as the tolerance toward impurities and their niche in stationary applications. However, the liquid 85% phosphoric acid inside a HT-PEMFC is not embedded in a silica matrix, which mitigates potential structural damage caused by the solidification of the 100% phosphoric acid in PAFCs [31–33].

Reference electrode setups are developed to further separate the impact of individual components of the impedance of the fuel cell. Mitsuda and Murahashi [34] employed multiple reference electrodes to investigate the impact of fuel starvation on the two electrodes separately. Li and Pickup [35] separated the anode and cathode potential by an edge-type reference electrode configuration along the lines of constant potential using a platinum wire. Kaserer et al. [36] implemented a bridge-type reference electrode by drilling a hole into the flow field and the gas diffusion electrode on the cathode side and connecting it via a salt bridge. Kuhn et al. [37] developed a one-dimensional cell setup in which the pseudo reference electrode was wire-shaped and embedded between two membranes.

A key analysis technique for evaluating the performance and the loss mechanisms in a PEMFC is the Electrochemical Impedance Spectroscopy (EIS), as it is recorded over a broad frequency range and records physicochemical phenomena occurring on different time scales [38–43]. The features of an impedance spectrum allow the differentiation between

individual components and operation parameters contributing to the losses inside a PEMFC. These parameters can be external, i.e. gas stoichiometry and applied current density, or internal, i.e. gas diffusion layer structure and catalyst layer structure, membrane and electrolyte resistance, reaction steps, and degradation [43–46]. Further, the losses inside a PEMFC can be investigated in greater detail. They are typically divided into Mass Transport (MT), Oxygen Reduction Reaction (ORR), and proton transport [47]. Andreasen et al. [48] showed that the proton transport and the anode processes, such as the hydrogen oxidation reaction, are fast and exhibit a low impedance compared to the cathode processes, such as oxygen MT and ORR. Yuan et al. [43] summarized the impact of various operation parameters on the impedance spectra of fuel cells.

However, without further analysis, EIS shows only qualitative information about the contribution of the individual cell components to the total cell impedance. The most dominant method to quantify each component of the spectrum is to employ an equivalent circuit model which entails the fuel cell components as electrical components, such as resistors, inductors, and capacitors [49]. Fitting the equivalent circuit to the impedance spectrum by assigning the electrical elements numerical values yields a quantitative insight into the impedance of fuel cell components. Niya and Hoorfar [41] discussed the benefits and the complications of the application of EIS equivalent circuit models and highlight the importance of a proper understanding of this method, as it can yield ambiguous results.

In 2002, Schichlein et al. [50] applied the convolution equation developed by Fuoss and Kirkwood [51] to impedance spectra of solid oxide fuel cells to successfully deconvolve the reaction mechanisms occurring on different time scales. Since then, the Distribution of Relaxation Times (DRT) method has been applied to various electrochemical systems [36,45,47,50,52–58]. Recently, Cuicci and Chen [59] developed a mathematical model based on a Bayesian approach, which entails the assumption that the response of the electrochemical system is a sum of relaxations of physicochemical processes in the system. This model allows the interpretation of experimentally obtained impedance spectra. DRTtools, a MATLAB-based tool kit, was applied in this work to perform the mathematical transformation of the EIS [60]. Weiß et al. [61] applied the DRT method using DRTtools to the HT-PEMFC and characterized the obtained fingerprint pattern of this electrochemical system by successfully allocating the peaks of the resulting DRT spectrum to loss mechanisms inside the fuel cell, such as MT, ORR, and faster, dominantly anodic processes such as proton transport and the hydrogen oxidation reaction.

In this study, HT-PEMFCs have been investigated using polarization curves, EIS, and DRT at various operation conditions. External parameters were systematically varied to have a better understanding of the features in the DRT spectra of HT-PEMFCs. A platinum mesh as a reference electrode, sandwiched between two membranes, is employed to separate the impedance of the anode from the cathode. We tested CO in the anode gas stream, nitrogen dilution, and reactant gas humidification. This investigation aims to gain a better understanding of the processes occurring in a HT-PEMFC and its influence on the DRT spectrum. A fundamental understanding of the DRT spectrum makes it a powerful tool to study the effect of varying operating conditions, degradation, and novel cell components on cell performance.

2. Methodology

2.1. Membrane Electrode Assembly fabrication

All cell tests were performed in a single cell setup. The Gas Diffusion Electrodes (GDE) were prepared by spray coating a catalyst ink layer by layer onto a commercially available Gas Diffusion Layer (GDL) with a microporous layer (H2315-C2, Freudenberg SE, Germany) using an airbrush system. The prepared ink consisted of a catalyst powder (20 wt-% Pt on Vulcan powder, Heraeus®, Germany), isopropyl alcohol,

deionized water, and a 60 wt-% Polytetrafluoroethylene (PTFE) dispersion (3 M™ Dyneon™, USA). The PTFE content amounted to 10% of the final Catalyst Layer (CL) weight. The ink was dispersed in an ultrasonic bath and subsequently sprayed onto the heated GDL to facilitate the evaporation of the solvents. The final loading amounted to 0.2 mgPt cm^{-2} on the anode and 1 mgPt cm^{-2} on the cathode. The loading was controlled by weighing the GDE during spray coating. The obtained GDE was cut into a square ($2 \text{ cm} \times 2 \text{ cm}$) placed onto a stainless steel bipolar plate containing a serpentine flow field. PTFE gaskets and Polyether Ether Ketone (PEEK) gaskets were used to control the compression of the GDE and to prevent leakage and gas crossover. A compression ratio of 25% of the total thickness of the GDE has been applied on each side. A PBI membrane (Dapozol® M40, Danish Power Systems, Denmark) doped in 85% phosphoric acid (H_3PO_4) for four weeks at room temperature was placed between the cathode and the anode GDE. A schematic of the cell setup is shown in Fig. 1, it shows the placement of the Pt mesh reference electrode between the PBI membranes. The preparation of the catalyst ink and the Membrane Electrode Assembly (MEA) is explained in greater detail in earlier work [62]. The cell was heated up to $160 \text{ }^\circ\text{C}$ and conditioned for three days in galvanostatic mode at 200 mA cm^{-2} until it reached a stable operating voltage. During this period, the stoichiometry of the gas flow amounted to $\lambda(\text{H}_2) = 1.8$ on the anode and $\lambda(\text{Air}) = 2.0$ on the cathode. From that point on, the operation parameters were varied depending on the individual experiment.

2.2. Impedance measurement and Distribution of Relaxation Times analysis

Impedance spectra have been recorded using a multichannel Zahner Zennium work station (Zahner Elektrik, Germany) at 300 mA cm^{-2} at a rate of 10 points per decade and 6 repetitions of each point. The frequency range was 100 kHz to 100 mHz and covers the whole range of interest, at which losses originating from proton transport, the ORR, and MT are occurring in the HT-PEMFC. The setup is shown in Fig. 1. Before

each measurement, an equilibration period of at least 30 min was included to ensure that the cell is in a stable operating condition.

The impedance data were subsequently analyzed using the Distribution of Relaxation Times analysis, which transforms the Nyquist plot from a real and imaginary impedance into a resistivity vs. frequency spectrum, which allows the separation and quantification of polarization losses occurring at different frequencies and time scales. No a priori knowledge of the intrinsic processes in the electrochemical device under study is necessary to convert a Nyquist plot using DRT, which presents an additional advantage over the equivalent circuit method, for which a detailed understanding of these processes is necessary before choosing an appropriate model which can accurately represent the device [38–42]. The input parameters of the DRT analysis applied in this work are determined by performing EIS on several circuits consisting of two known electrical Resistor-Capacitor (RC) elements in series. The resulting DRT method was able to accurately resolve the resistance and capacity of each resistor or capacitor, respectively. The impedance of an RC element can be obtained by integration over the respective DRT peak.

Weiß et al. [61] obtained a set of parameters by fitting DRT spectra to known RC elements and successfully applied it to a HT-PEMFC, which allowed for the allocation of each resulting peak to a loss mechanism of the fuel cell. This set of parameters is further applied in this work. The Nyquist plot (also referred to as the impedance or the electrochemical impedance spectrum, EIS) and the resulting DRT spectrum of a HT-PEMFC are shown in Fig. 2 b) and 2 c). The impedance spectrum exhibits multiple processes, indicated by a colored semi-circle in Fig. 2 b). The impedance of these processes overlaps to result in mainly three discernable arcs, which can be distinguished by eye. These arcs are allocated to MT (Arc 1), the ORR (Arc 2), and the high-frequency processes, including proton transport in the catalyst layer and the hydrogen oxidation reaction (HOR) (Arc 3).

The DRT method can break down each contribution to the impedance spectrum and displays each process by a peak in the DRT spectrum,

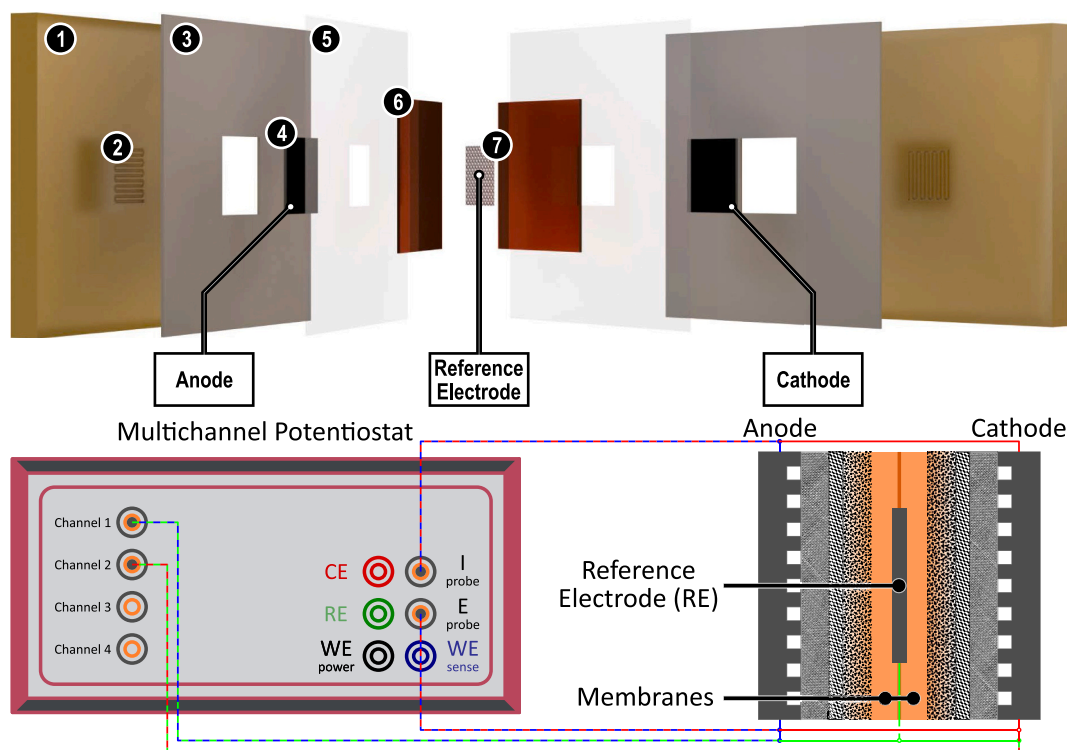


Fig. 1. Schematic representation of the setup of the cell containing a reference electrode (Pt mesh). (1) bipolar plate, (2) serpentine flow field, (3) PTFE gasket, (4) Pt electrode, (5) PEEK subgasket, (6) doped PBI membrane, (7) reference electrode. The reference electrode was placed between two doped PBI membranes to avoid electrical contact with the electrodes.

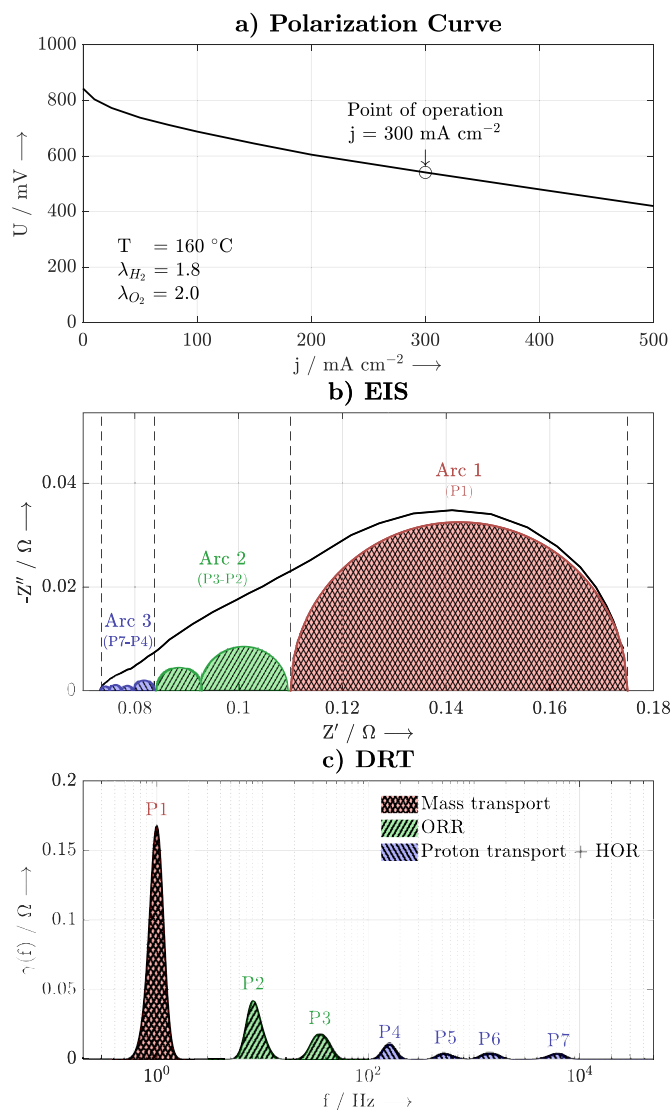


Fig. 2. a) Polarization curve of the investigated HT-PEMFC. The impedance spectra were recorded at 300 mA cm^{-2} . b) Nyquist plot showing the impedance spectrum. Arc 1 represents the MT (red), Arc 2 shows the frequencies at which the ORR occurs (green) and Arc 3 includes the high-frequency regime (blue). c) DRT spectrum resulting from the EIS of the fuel cell. The coloration of the peaks corresponds to the arcs in the Nyquist plot. (For interpretation of the references to color in this figure legend, the reader is referred to the Web version of this article.)

however, an overlap may occur. Weiß et al. [61] allocated each peak to processes occurring in a HT-PEMFC by systematically varying the operation parameters and observing the effect on the DRT spectrum. Following their findings, the peaks in Fig. 2 c) can be attributed as follows: MT (P1), ORR (P2, P3), high frequency (P4-P7). This method allows the quantification of each loss in the fuel cell and the quantification of the impact of varying operation parameters during operation and is a valuable tool to understand the processes inside a HT-PEMFC. When recording the low-frequency part of the EIS, local oscillations of the oxygen concentration on the cathode side can occur. The concentration along the flow channels can fluctuate due to the slow and repeating change of the current density [63–66]. This is not expected in our cell setup, as the dimensions of the single-cell are too small to create these local oscillations at a stoichiometry of $\lambda(\text{Air}) = 2.0$. Further, the oxygen mass transport inside a HT-PEMFC catalyst layer can be approximated by an RC element, as the diffusion is slower than in a LT-PEMFC. At higher diffusion rates, a Warburg element is necessary to accurately

depict the diffusion processes. Further differences to the LT-PEMFC are included in the architecture and design. Most notably the PEM itself. Instead of a Nafion membrane hydrated with water, the HT-PEMFC employs a PBI membrane doped with concentrated phosphoric acid as the electrolyte. As the proton conduction in a HT-PEMFC is carried out by the phosphoric acid, the triple-phase boundary is dynamic and changes during operation. A higher current density increases the water content in the cathode and as such, in the phosphoric acid inside the cathode and leads to a change in viscosity and contact angle of the electrolyte [67]. A suboptimal distribution of phosphoric acid can be expected in a HT-PEMFC catalyst layer and is currently under investigation by various groups [68–77]. The increased thickness of the catalyst layer aggravates the impact of a not ideal electrolyte distribution and increases the length of the diffusion path of oxygen, which results in a larger MT loss occurring at a time scale at approximately 1 Hz instead of 10 Hz, as this is the case in LT-PEMFCs [28]. Further, a non-uniform electrolyte distribution is coupled with the thickness of the CL and results in several high-frequency peaks, as seen in Fig. 2 c). They were mainly attributed to proton transport in the CL. It is known that phosphoric acid adsorbs onto the platinum catalyst and therefore hampers the ORR in HT-PEMFCs. Consequently, the DRT spectrum displays two peaks linked to the complex process of the ORR in hot phosphoric acid [61] which is not observed for LT-PEMFCs [47].

3. Results & discussion

3.1. Effect of humidification

Humidification in a fuel cell is of importance, as the increased amount of water in the cell changes the concentration of phosphoric acid inside the electrode, which alters the wetting properties such as contact angle and the viscosity of phosphoric acid inside the porous electrode [78]. These effects can be expected to have an impact on the impedance spectra and the resulting DRT analysis. To investigate the impact of gas humidification, fuel cells were operated at varying levels of Relative Humidity (RH) of the anode gas. The humidifier was set to dew points of 40 °C ($\text{RH} = 1.2\%$) and 60 °C ($\text{RH} = 3.2\%$) to investigate the effect of reactant gas humidification. The low relative humidity simulates the amount of water vapor present in a hydrogen stream obtained from industrial processes. It is known, that humidification of the gases is leaching the acid out of the GDE which causes severe cell degradation and bipolar plate corrosion over time [77,79,80]. However, the experiments with increased humidification were carried out within a time frame of three hours and this effect could, therefore, be neglected.

Fig. 3 shows the performance and the analysis of fuel cells operated at different levels of anode inlet gas humidification. In Fig. 3 a), the polarization curves of the cells are compared. No apparent impact of humidity on the performance can be seen at an RH of 3.2% and below. Above 100 mA cm^{-2} , the voltage difference between the levels of RH amounts to less than 2 mV. The impedance spectra are shown in Fig. 3 b). The impedance of the cell increases throughout the whole frequency range and the increase is slightly more pronounced at lower frequencies, e.g. MT and ORR. However, the net increase of the impedance is still small, amounting to 1.1% for the MT for and 1.1% for the ORR impedance at 3.2% RH. These numbers were extracted from the DRT spectra in Fig. 3 c). The spectra show, that the position of the peaks remains stable when varying the relative humidity and the area under the curve shows only minor variations, which leads to the conclusion that the nature of these processes remains the same. However, two peaks at high frequency (P5 & P6, displayed in the zoom-in Fig. 3 c) change under humidification. We thus hypothesize that these peaks are linked to the distribution of phosphoric acid, as the humidification impacts the acid household of the cell, specifically that of the GDE. Slight variations of the acid composition and acid distribution in the CL are mainly affecting the high-frequency range of the DRT spectrum, as seen in P5 & P6 in Fig. 3 c), since it is linked to the proton conductivity of the CL. In

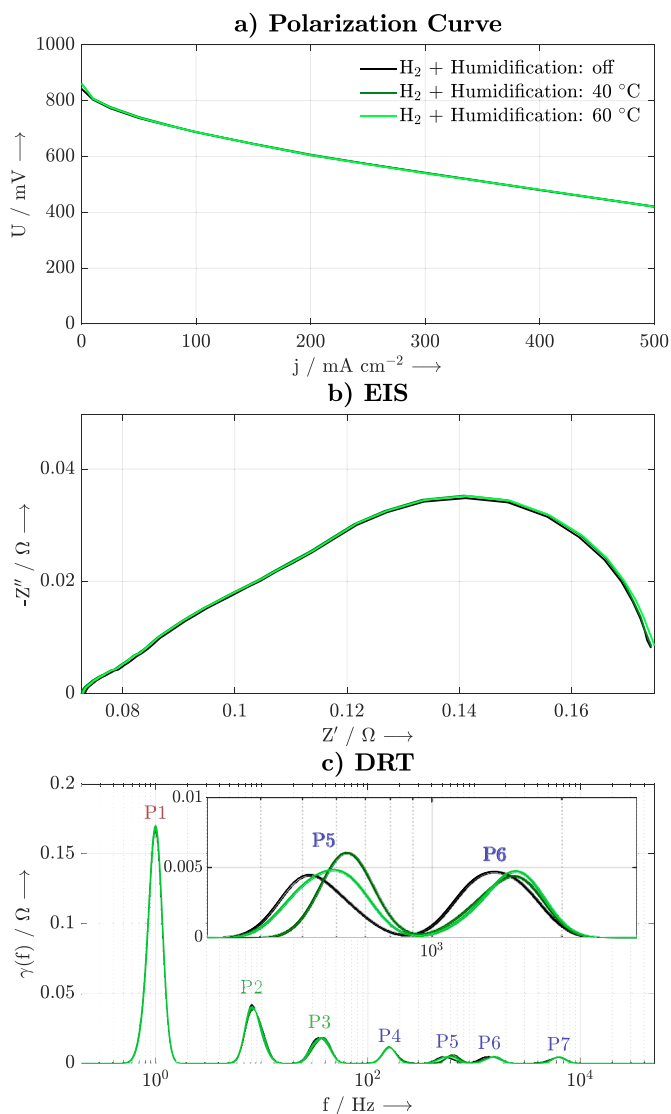


Fig. 3. Comparison of performance of HT-PEM fuel cell at three levels of RH (black: 0.0% RH, dark blue: 1.2% RH, light blue: 3.2% RH) in the anode inlet gas using (a) polarization curve, (b) Nyquist plot, and (c) DRT analysis. (For interpretation of the references to color in this figure legend, the reader is referred to the Web version of this article.)

this case, the composition of phosphoric acid changes due to the higher water content of the MEA and, therefore, alters the wetting properties of the acid. This changes the proton transport of the electrode (P5 & P6 in the DRT spectrum) to a small degree, but not enough to deteriorate the performance significantly. Such details are only visible in the DRT spectrum and cannot be observed in the Nyquist plot.

3.2. Effect of nitrogen dilution

Fig. 4 compares the performance of the HT-PEMFC when operated at different levels of anode inlet gas dilution. The dilution was achieved by mixing nitrogen gas (10 vol-%, 20 vol-%, all following gas mixing levels are given in vol-%) into the anode gas stream. Fig. 4 displays the impact of nitrogen dilution on performance and impedance. It can be observed that 10% of N₂ already leads to a small decrease in performance throughout the whole range of current densities. This decrease amounts to 2 mV at the Open Circuit Voltage (OCV) and below 100 mA cm⁻² and increases to 3 mV above 100 mA cm⁻². This effect is enhanced when mixing 20% nitrogen in the anode gas stream, leading to a voltage

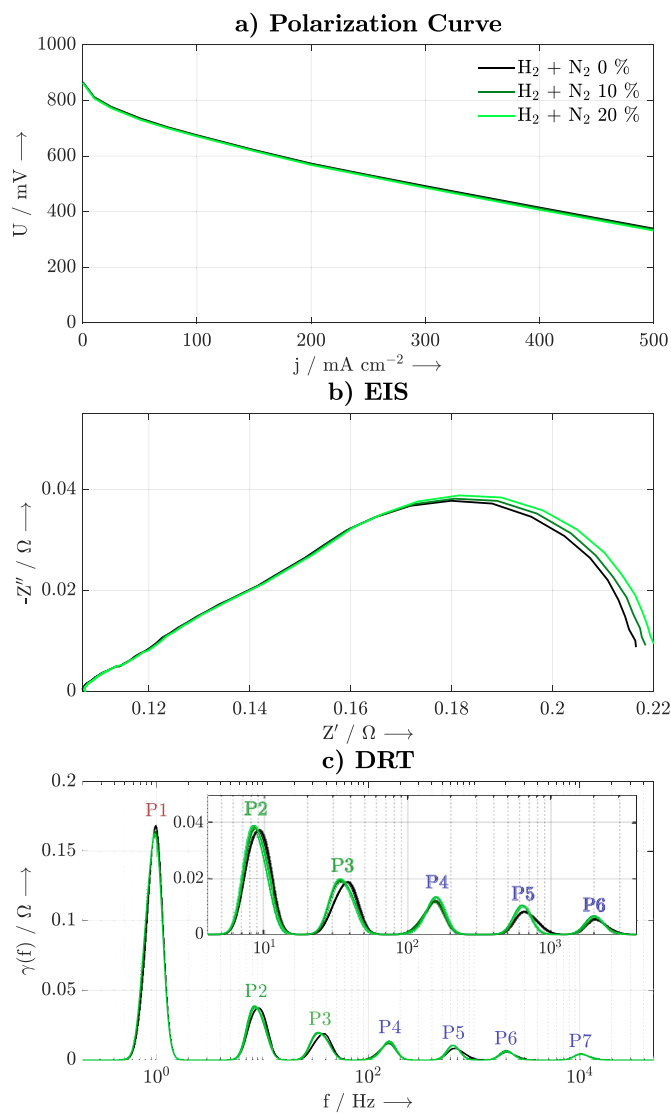


Fig. 4. Comparison of performance of HT-PEM fuel cell at three levels of nitrogen dilution (black: 0% N₂, orange: 10 vol-% N₂, yellow: 20 vol-% N₂) of the anode inlet gas using (a) polarization curve, (b) Nyquist plot, and (c) DRT analysis. (For interpretation of the references to color in this figure legend, the reader is referred to the Web version of this article.)

difference of 4 mV at OCV and increases to 5–6 mV above 100 mA cm⁻². The voltage decrease caused by dilution at the open circuit potential can be approximated by the Nernst equation if the activity of the anodic ions is replaced by the relative partial pressure. It predicts a voltage decrease of 2 mV at 10%, and 4 mV at 20% N₂ dilution, which agrees perfectly with the measured OCV data.

The impedance is shown in Fig. 4 b) and highlights that the nitrogen dilution mainly affects the lower frequencies. This is verified by DRT analysis, which can resolve the contribution of ORR and MT separately. Integration of the peaks attributed to the MT results in an increase of 1.5% MT resistance at 10% N₂ in the gas stream and a 3.0% increase at 20% N₂. The increase of the ORR amounts to 1.3% at 10% N₂ and 2.4% at 20% N₂. As the MT resistance dominates the total cell impedance, the net increase of the MT resistance is impacting the cell more strongly than the net increase of the ORR resistance. As the nature of all processes in the cell remains typically the same during the nitrogen dilution, only little changes are observed in the DRT spectrum. This is especially true for the low-frequency peak attributed to MT, the position of which remains stable during the whole experiment. However, a shift toward

lower frequencies is observed for the peaks allocated to the ORR. We assume that this shift originates from the decreased potential of the fuel cell. The exchange current density of the ORR is dependent on the electrode potential. As N_2 is introduced, the voltage of the cell decreases, which in turn decreases the exchange current density of the ORR according to Butler-Volmer. In the EIS measurement, this leads to a higher detected ORR resistance and this translates into a shift in the DRT spectrum toward lower frequencies and a larger area under the peak, corresponding to higher resistance. As the total cell voltage changes only little when N_2 is mixed into the gas stream, the shift in the DRT spectrum is therefore small as well.

3.3. Effect of carbon monoxide poisoning

Fig. 5 shows the impact of 1% and 2% CO in the anode gas stream on HT-PEM fuel cells. As expected, already small quantities of CO show a significant impact on the performance of the fuel cell. This effect outweighs the impact of humidification and nitrogen dilution, which shows that it is not dominated by the dilution and the decrease of the partial

pressure of hydrogen in the anode. Fig. 5 a) compares the voltage of the fuel cell operated with 0%, 1%, and 2% CO in the anode gas stream. To enhance the impact of CO on the cell, the platinum loading in the anode was reduced to 0.2 mgPt cm^{-2} . A lower platinum content decreases the CO tolerance of the cell, as the partial coverage of active catalyst sites even further reduces the number of free sites. Since the exchange current density j_0 of the HOR is dependent on the number of free catalytic sites, the lower anodic platinum content deteriorates the cell performance even more in the presence of CO. The usually expected CO tolerance ($<10 \text{ mV}$ voltage loss) of a HT-PEMFC of up to 5% is not given at a low loading of 0.2 mgPt cm^{-2} . At the operating current of 300 mA cm^{-2} , the cell exhibits a voltage of 492 mV . The addition of 1% CO leads to a voltage decrease of 29 mV . For 2% CO, the decrease amounts to 44 mV , which amounts to almost 10% of the total cell voltage.

The Nyquist plots in Fig. 5 b) show that all frequency regions are affected by CO poisoning, specifically, the frequency midrange of the DRT allocated to the ORR. Similar effects have also been observed in previous studies in which they were interpreted differently [28,81]. For example, Andreasen et al. [28] have them attributed to longer diffusion paths of hydrogen through the anode catalyst layer (increased impedance at 100 Hz) and local oscillations of hydrogen concentration in the anode, extending into the channels of the flow field ($<100 \text{ Hz}$). Further, the addition of CO in the anode gas is expected to increase the half-cell potential, similar to hydrogen starvation. The anode potential increases to a point at which the carbon oxidation reaction and the carbon monoxide oxidation may occur, as well as the water electrolysis in extreme cases [82–84]. Yezerska et al. [85] observe an additional peak arising in the DRT between 300 Hz and 800 Hz after hydrogen starvation and allocate it to potential side reactions. To investigate these explanations, a cell setup using a reference electrode was used in this work. This way, the contribution of cathode and anode could be separated and the origin of the increased impedance is shown.

3.4. Reference electrode setup

By implementing a platinum mesh as a reference electrode within the MEA, the electrochemical reaction of anode and cathode could be investigated independently from each other. The reference electrode was placed between two doped PBI membranes to avoid electrical short circuits. Due to the presence of Pt (platinum mesh), an acid reservoir (proton conductor) and hydrogen (hydrogen crossover through the membrane) a dynamic reference electrode was created. This specific fuel cell was equipped with two membranes but otherwise operated normally. The Nyquist plot of the impedance measurements in which the electrodes were connected to the work station separately is shown in Fig. 6 a). The contribution of the anode to the total cell impedance amounts to 2%, excluding the membrane resistance. This is a small fraction compared to the cathode contribution, which leads to the conclusion that the cathode processes, such as the oxygen transport inside the cathode CL and the ORR dominate the impedance of the full cell. Furthermore, the anode and cathode impedance spectra add up to the full cell spectrum. So the method can separate the anode from the cathode processes which allows us a more detailed analysis of each of them. An inductive contribution was observed in the high-frequency part of the Nyquist plot of the anode, which was omitted in Fig. 6, as it is believed to originate from the setup instead of being caused by the fuel cell. However, it is part of the mathematical summation and part of the full cell spectrum in the Nyquist plot. The DRT only includes values in the fourth quadrant (y-axis is negative in Fig. 6 a) of the Nyquist plot, which is why the inductive part is omitted in the DRT spectrum in Fig. 6 b), as we only see the impedance of the fourth quadrant in the DRT spectrum. Hence, the mathematical summation appears similar to the cathode spectrum, instead of the full cell spectrum, which highlights the small influence of the anode compared to the cathode. This is expected to be closer to the real cell, as the influence of the setup is not part of the spectrum.

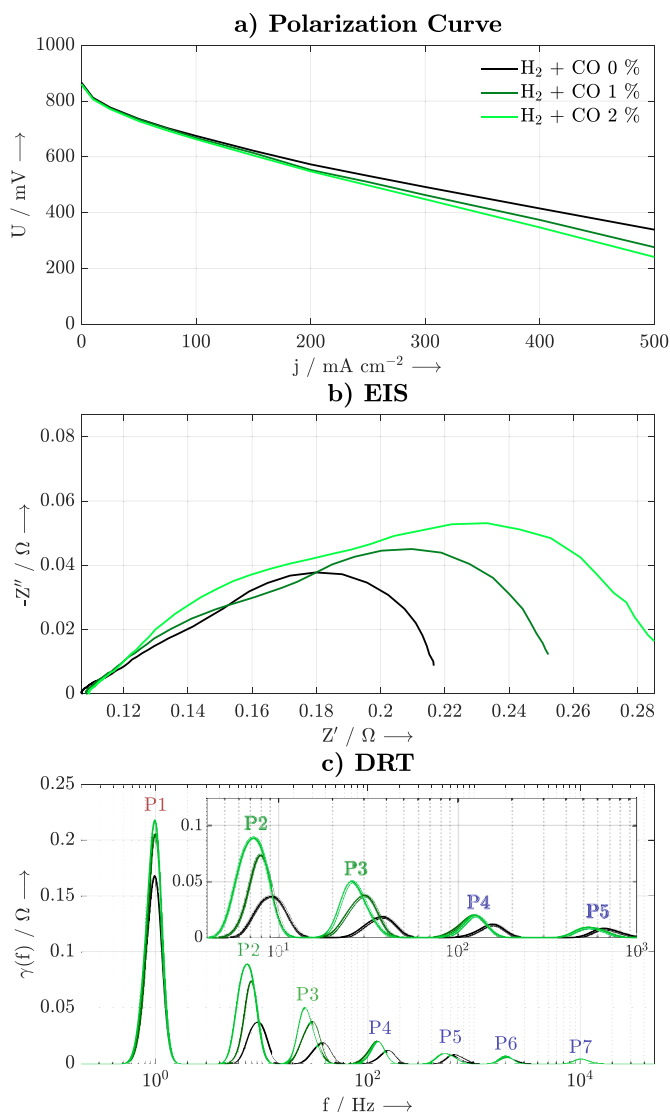


Fig. 5. Comparison of performance of HT-PEM fuel cell at three levels of CO contamination (black: 0 vol-% CO, dark green: 1 vol-% CO, light green: 2 vol-% CO) of the anode inlet gas using (a) polarization curve, (b) Nyquist plot, and (c) DRT analysis. (For interpretation of the references to color in this figure legend, the reader is referred to the Web version of this article.)

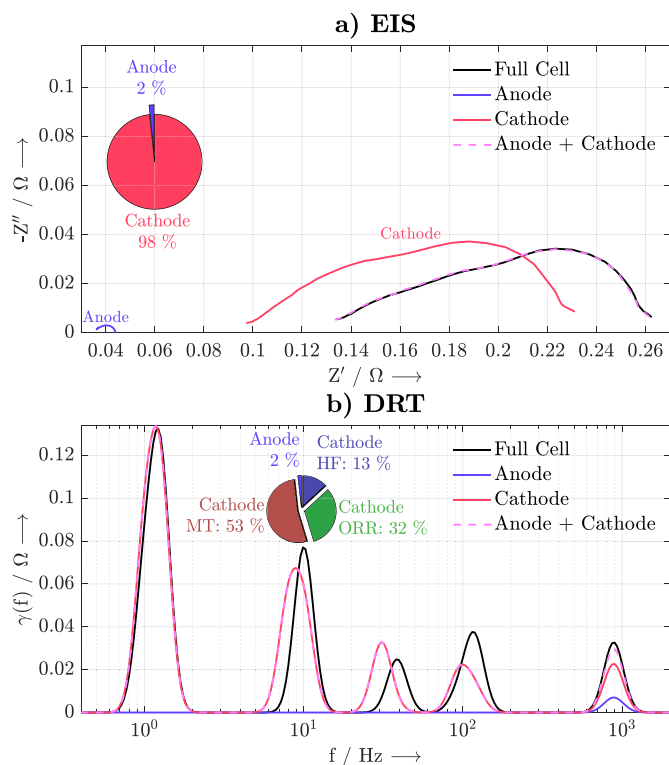


Fig. 6. (a) Nyquist plot and (b) DRT analysis of the impedance recorded using the reference cell setup with a dynamic reference electrode. Pie charts display the individual shares of the polarization contributions.

The DRT of the anode exhibits only one single peak at high frequencies, at 1 kHz, as the result of one round semi-circle in the EIS. We assume this peak is associated with charge transfer of the HOR occurring at the anode electrode. With platinum as a catalyst, the HOR is straightforward and kinetically fast, therefore only a tiny single peak at 1 kHz is visible in the DRT spectrum. On the anode, no MT limitations are observed since there is any peak present in the low-frequency regime.

The breaking of the oxygen-oxygen bond on the surface of platinum does not occur as readily as for the hydrogen molecule. Generally, the ORR process is much more complex, it requires many individual steps and significant molecular reorganization than that of the HOR. The exchange current densities for the ORR are usually at least six orders of magnitude lower than for the HOR [86]. Especially, in the case of the HT-PEMFC, where also specific adsorption of the electrolyte further hampers the reaction kinetics. Additionally, the air supply, a mixture of oxygen and nitrogen, creates transport losses through the GDE, thus a large peak at 1 Hz appears in the DRT spectrum of the cathode. Because of its complexity, the cathode process generates nearly all polarization contributions of the entire cell (98%), whereas the anode only contributes 2% to the total impedance.

3.5. Effect of carbon monoxide poisoning measured with reference electrode setup

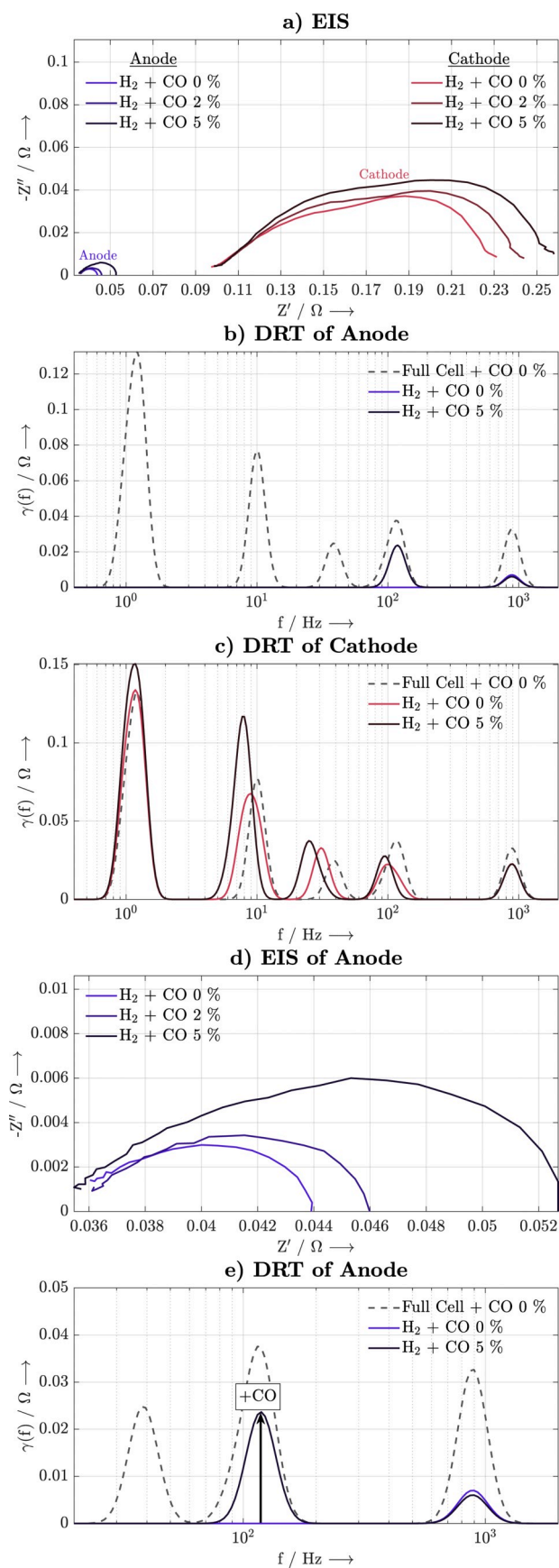
As shown in Fig. 7 a) the impedance of the anode and the cathode increases in the presence of CO impurities in the hydrogen stream. Interestingly, the anode not only increases its size but also its general shape, from a perfect semi-circle into an elongated arc. The DRT analyses transform a single semi-circle into one peak at 1 kHz and the elongated arc into two peaks at 1 kHz and 100 Hz (see Fig. 7 b, d, e). As already described in Section 3.4, with pure hydrogen as fuel the HOR is simplistic and kinetically fast. If CO is added into the hydrogen stream the anode kinetics become more complex and sluggish. The presence of

CO generates undesirable side reactions such as the adsorption of CO onto the platinum surface, blocking the active catalytic sites. This effect could explain the appearance of a second peak at 100 Hz in the DRT spectrum once traces of CO are present in the gas feed. The time scale suggests that the process is most likely related to a charge-transfer on the electrode surface. Additionally, the water gas shift reaction may occur in the presence of water, which is introduced into the anode catalyst layer by concentrated phosphoric acid (85%) [81]. Andreasen et al. [28] observed in their experiments also that the impedance of an HT-PEMFC increase at around 100 Hz when CO is present on the anode. They interpreted this effect with a larger diffusion pathway of hydrogen due to the active sites being blocked with adsorbed CO. However, we expect a gas transport-related process to occur at lower frequencies. Yet, to prove this assumption highly sophisticated gas inlet and outlet analyses would be needed which is beyond the scope of this study.

Additionally, Andreasen et al. [28] further conclude that at even lower frequencies (<10 Hz), the local variations in H₂ concentration extend into the gas channel as described by various groups [63–66]. This phenomenon is not visible in the reference electrode setup, in which the anode does not exhibit any impedance at frequencies higher than 100 Hz, even at high CO concentrations of 5%. It is important to note that oscillations inside the gas channel at low frequencies may occur in a cell setup with a larger active area and thus longer gas channels. In a 2 × 2 cm active area and a hydrogen stoichiometry of λ(H₂) = 1.8, as was used in this work, no such concentration fluctuations are observed.

The cathode impedance is much larger (as mentioned earlier, 98% of the total cell impedance arises from the cathode) compared with that of the anode. The cathode impedance exhibits multiple arcs, at least three are visible in the Nyquist plot. CO in the anode gas inlet causes also the arcs of the cathode impedance to increase. The increase is only visible at the mid and low-frequency region (<100 Hz), which are attributed to the ORR and the MT of the cell [61], the high-frequency arc remains nearly unchanged. The cathode is primarily responsible for the increase of the entire cell impedance as seen in Figs. 5 and 7 and described in previous publications [28,81–85]. This proves that the anode processes are linked to the cathode. It is somehow counter-intuitive that cathode impedance is severely affected when only the gas flow is altered on the anode. The frequency region associated with the ORR is distinct and growing with increasing CO concentrations. No increase of the impedance of the anode at the ORR frequencies (3 Hz < f_{ORR} < 70 Hz) is observed, which leads to the conclusion that the ORR on the cathode is impacted by the presence of CO in the anode gas stream. The crossover of CO through the membrane to the cathode side cannot account for the ORR polarization loss [87,88]. The cathode potential is too high that CO adsorbs onto the platinum surface. We assume the reason for the hampered ORR lies again in the increased anode potential which leads to a lower cell voltage. At 300 mA cm⁻² and 5% CO, an anode potential (between the anode and the reference electrode) of 102 mV was observed. The cell voltage dropped by 44 mV, which decreases the cathode potential by 58 mV. The potential difference in the cathode leads to an exponential drop in the exchange current density governed by the Butler-Volmer equation. This dependence of the exchange current density is exponential to the potential shift and thus, the reaction seems to be severely hampered, leading to a significantly higher impedance at these frequencies.

The same effect also applies to the impedance of the MT regime. A change of the cell potential due to the flow of CO in the hydrogen gas feed also alters the impedance of MT since the current is fixed in galvanostatic EIS mode. Only in this case, the MT impedance is equivalent to an RC element. At low frequency, the impedance of the RC element is given by the resistor following Ohm's law. As anode voltage increases (the cell voltage drops), the MT appears larger as seen in the DRT analyses of Fig. 7 c. The total cell impedance can be generated within series-connected impedance elements of various types representing different cell processes that follow the principle of a potential divider.



(caption on next column)

Fig. 7. Impedance obtained from the cell containing the reference electrode from 0% CO to 5% CO in the anode gas stream. (a) Nyquist plots of anode and cathode, (b) DRT spectra of the anode, obtained from the Nyquist plots in (a), (c) DRT spectra of the cathode, obtained from the Nyquist plots in (a), (d) Zoomed-in Nyquist plot of the anode from (a), (e) Zoomed-in DRT spectrum of the anode. The DRT spectra of 2% CO in the anode gas stream are omitted for clarity.

4. Conclusions

In this work, the impedance of a HT-PEMFC has been investigated thoroughly using the Distribution of Relaxation Times analysis and the influence of parameters such as humidification, anode gas stream dilution with nitrogen and the presence of CO up to 5% in the anode fuel have been explored. To understand the observed variations, a reference electrode was introduced to separate the anode impedance from the cathode impedance.

Humidification of the fuel did not affect the HT-PEMFC performance. The shape of the Nyquist plot did not change much, which indicates that the nature of the processes inside the fuel cell does not change significantly up to a value of 3.2% relative humidity. Humidification affects the dilution of phosphoric acid, which changes high-frequency peaks in the DRT spectrum. Thus, these peaks can be allocated to the proton transport in the catalyst layers. Other peaks in the DRT spectrum remain unaltered.

Nitrogen dilution of the anode gas stream of up to 20 vol-% decreases the performance of the fuel cell by 5 mV at 300 mA cm⁻². The decrease of the OCV at 10 vol-% and 20 vol-% N₂ amounts to 2 mV and 4 mV respectively. This matches the theoretically expected decrease using the Nernst equation. The dilution effect leads to a slight deviation in the shape of the Nyquist plot at low frequencies. DRT showed a minor increase of 3.0% in the MT resistance of oxygen as well as an increase of 2.4% in the ORR resistance at 20 vol-% N₂. This increase can be explained by the principle of a potential divider. As the voltage of the fuel cell decreases, the measured impedance increases for these ohmic processes. Thus, the impact of changing the anode fuel stream on the cathode processes can be explained.

The introduction of 2% and 5% CO in the anode gas stream strongly impacted the fuel cell performance. At 300 mA cm⁻² and an anode platinum loading of 0.2 mgPt cm⁻², the voltage dropped by 29 mV with 2% CO impurities and 44 mV with 5% CO on the anode side. This huge influence of CO is visible in the Nyquist plot of the fuel cell. The typical three arcs visible in a HT-PEMFC Nyquist plot grew a lot more distinct in the presence of CO. The main difference was observed in the middle frequency part (3 Hz–70 Hz), typically attributed to the ORR and at lower frequencies, attributed to the MT of the cell. However, the presence of CO affects the EIS at all frequencies. To clarify the impact of CO on the anode and the cathode separately, a dynamic reference electrode has been introduced into the fuel cell.

The separation of anode and cathode EIS showed that without CO, the anode exhibits only one single DRT peak at 1 kHz. The total contribution of the anode EIS amounts to 2% of the total cell impedance. Adding CO causes a second peak to arise in the DRT spectrum of the anode, at lower frequencies of 100 Hz. However, no impedance originates from the anode at even lower frequencies, which indicates that diffusion processes are not affected by the addition of CO. Thus, the impact of CO at lower frequencies than 100 Hz originates solely from the cathode. The ORR on the cathode side is hampered as the half-cell potential of the cathode drops by 58 mV when 5% CO is introduced. The reaction can be described by the Butler-Volmer equation. If the voltage drops, the exchange current density drops exponentially, resulting in a higher observed impedance. The changes in the MT in the presence of CO are linked to the principle of a potential divider, as the behavior of the RC element describing the MT can be approximated to follow Ohm's law. Here again, the lower cell potential is the cause of the increased measured impedance at low frequencies and neither an actual increase

in the MT resistance nor cross-over of CO.

Declaration of competing interest

The authors declare that they have no known competing financial interests or personal relationships that could have appeared to influence the work reported in this paper.

CRedit authorship contribution statement

N. Bevilacqua: Formal analysis, Data curation, Writing - original draft. **M.A. Schmid:** Investigation, Visualization. **R. Zeis:** Conceptualization, Writing - review & editing, Funding acquisition, Supervision.

Acknowledgments

Financial support from the “Impuls-und Vernetzungsfonds der Helmholtz Gesellschaft” (Young Investigator Group Project VH-NG-616) is greatly acknowledged. Further, the authors would like to thank the ZSW (Zentrum für Sonnenenergie und Wasserstoff-Forschung) for providing the facility and the resources for fuel cell operation. This work contributes to the research performed at CELEST (Center for Electrochemical Energy Storage Ulm-Karlsruhe).

Glossary

CL	Catalyst Layer
DRT	Distribution of Relaxation Times
EIS	Electrochemical Impedance Spectroscopy
f	Frequency (variable)
GDE	Gas Diffusion Electrode
GDL	Gas Diffusion Layer
H ₂	Hydrogen
H ₃ PO ₄	Phosphoric Acid
HT-PEMFC	High-Temperature Polymer Electrolyte Membrane Fuel Cell
LT-PEMFC	Low-Temperature Polymer Electrolyte Membrane Fuel Cell
MEA	Membrane Electrode Assembly
MT	Mass Transport
N ₂	Nitrogen
ORR	Oxygen Reduction Reaction
PBI	Polybenzimidazole
PEEK	Polyether ether ketone
Pt	Platinum
PTFE	Polytetrafluoroethylene
RC	Resistor-Capacitor
RH	Relative Humidity

References

- Q. Li, J.O. Jensen, R.F. Savinell, N.J. Bjerrum, High temperature proton exchange membranes based on polybenzimidazoles for fuel cells, *Prog. Polym. Sci.* 34 (2009) 449–477.
- S.S. Araya, F. Zhou, V. Liso, S.L. Sahlin, J.R. Vang, S. Thomas, X. Gao, C. Jeppesen, S.K. Kær, A comprehensive review of PBI-based high temperature PEM fuel cells, *Int. J. Hydrogen Energy* 41 (2016) 21310–21344.
- A. Chandan, M. Hattenberger, A. El-kharouf, S. Du, A. Dhir, V. Self, B.G. Pollet, A. Ingram, W. Bujalski, High Temperature (HT) polymer electrolyte membrane fuel cells (PEMFC) - a review, *J. Power Sources* 231 (2013) 264–278.
- R.K.A. Rasheed, Q. Liao, Z. Caizhi, S.H. Chan, A review on modelling of high temperature proton exchange membrane fuel cells (HT-PEMFCs), *Int. J. Hydrogen Energy* 42 (2017) 3142–3165.
- R.E. Rosli, A.B. Sulong, W.R.W. Daud, M.A. Zulkifley, T. Husaini, M.I. Rosli, E. H. Majlan, M.A. Haque, A review of high-temperature proton exchange membrane fuel cell (HT-PEMFC) systems, *Int. J. Hydrogen Energy* 42 (2017) 9293–9314.
- M.G. Waller, W.M. R, T.A. Trabold, Performance of high temperature PEM fuel cell materials. Part 1: effects of temperature, pressure and anode dilution, *Int. J. Hydrogen Energy* 41 (2016) 2944–2954.
- R. Zeis, Materials and characterization techniques for high-temperature polymer electrolyte membrane fuel cells, *Beilstein J. Nanotechnol.* 6 (2015) 68–83.
- S. Chevalier, J. Lee, N. Ge, R. Yip, P. Antonacci, Y. Tabuchi, T. Kotaka, A. Bazylak, In operando measurements of liquid water saturation distributions and effective diffusivities of polymer electrolyte membrane fuel cell gas diffusion layers, *Electrochim. Acta* 210 (2016) 792–803.
- S.G. Kandlikar, Microscale and macroscale Aspects of water management challenges in PEM fuel cells, *Heat Tran. Eng.* 29 (2008) 575–587.
- S.G. Kandlikar, Two-phase flow in GDL and reactant channels of a proton exchange membrane fuel cell, *Int. J. Hydrogen Energy* 39 (2014) 6620–6636.
- H. Li, Y. Tang, Z. Wang, Z. Shi, S. Wu, D. Song, J. Zhang, K. Fatih, J. Zhang, H. Wang, Z.-S. Liu, R. Abouatallah, A. Mazza, A review of water flooding issues in the proton exchange membrane fuel cell, *J. Power Sources* 178 (2008) 103–117.
- A.Z. Weber, R.L. Borup, R.M. Darling, P.K. Das, T.J. Dursch, W. Gu, D. Harvey, A. Kusoglu, S. Litster, M.M. Mench, R. Mukundan, J.P. Owejan, J.G. Pharoah, M. Secanell, I.V. Zenyuk, A critical review of modeling transport phenomena in polymer-electrolyte fuel cells, *J. Electrochem. Soc.* 161 (2014) F1254–F1299.
- N. Zamel, X. Li, Effect of contaminants on polymer electrolyte membrane fuel cells, *Prog. Energy Combust. Sci.* 37 (2011) 292–329.
- Q. Li, R. He, J.-A. Gao, J.O. Jensen, N.J. Bjerrum, The CO poisoning effect in PEMFCs operational at temperatures up to 200 °C, *J. Electrochem. Soc.* 150 (2003) A1599–A1605.
- C. Zhang, W. Zhou, M.M. Ehteshami, Y. Wang, S.H. Chan, Determination of the optimal operating temperature range for high temperature PEM fuel cell considering its performance, CO tolerance and degradation, *Energy Convers. Manag.* 105 (2015) 433–441.
- S.K. Das, A. Reis, K.J. Berry, Experimental evaluation of CO poisoning on the performance of a high temperature proton exchange membrane fuel cells, *J. Power Sources* 193 (2009) 691–698.
- S.S. Araya, S.J. Andreasen, S.K. Kær, Experimental characterization of the poisoning effects of methanol-based reformat impurities on a PBI-based high temperature PEM fuel cell, *Energies* 5 (2012) 4251–4267.
- K. Oh, H. Ju, Temperature dependence of CO poisoning in high-temperature proton exchange membrane fuel cells with phosphoric acid-doped polybenzimidazole membranes, *Int. J. Hydrogen Energy* 40 (2015) 7743–7753.
- D.C. Seel, B.C. Benicewicz, L. Xiao, T.J. Schmidt, High-temperature Polybenzimidazol-Based Membranes, *Handbook of Fuel Cells*, John Wiley & Sons, Ltd, 2010.
- N.R.E. Laboratory, 1 - 10 kW Stationary Combined Heat and Power Systems Status and Technical Potential, National Renewable Energy Laboratory, 2010.
- A.H. Mamaghani, B. Najafi, A. Casalegno, F. Rinaldi, Predictive modelling and adaptive long-term performance optimization of an HT-PEM fuel cell based micro combined heat and power (CHP) plant, *Appl. Energy* 192 (2017) 519–529.
- S. Pasupathi, C.J.C. Gomez, H. Su, H. Reddy, P. Bujlo, C. Sita, Stationary HT-PEMFC-based systems - combined heat and power generation, in: B. Pollet (Ed.), *Recent Advances in High-Temperature PEM Fuel Cells*, Academic Press, 2016, pp. 55–77.
- A. Haryanto, S. Fernando, N. Murali, S. Adhikari, Current status of hydrogen production techniques by steam reforming of ethanol: a review, *Energy Fuels* 19 (2005) 2098–2106.
- C. Wu, R. Liu, Sustainable hydrogen production from steam reforming of bio-oil model compound based on carbon deposition/elimination, *Int. J. Hydrogen Energy* 36 (2011) 2860–2868.
- B. Zhang, X. Tang, Y. Li, Y. Xu, W. Shen, Hydrogen production from steam reforming of ethanol and glycerol over ceria-supported metal catalysts, *Int. J. Hydrogen Energy* 32 (2007) 2367–2373.
- S. Czernik, R. Evans, R. French, Hydrogen from biomass-production by steam reforming of biomass pyrolysis oil, *Catal. Today* 129 (2007) 265–268.
- F. Barbir, *PEM Fuel Cells: Theory and Practice*, Elsevier Inc, 2013.
- S.J. Andreasen, J.R. Vang, S.K. Kær, High temperature PEM fuel cell performance characterisation with CO and CO₂ using electrochemical impedance spectroscopy, *Int. J. Hydrogen Energy* 36 (2011) 9815–9830.
- J. Chen, J.B. Siegel, A.G. Stefanopoulou, Nitrogen blanketing from equilibria in dead end anode fuel cell operation, in: *Proceedings of the 2011 American Control Conference*, 2011.
- Q. Meyer, S. Ashton, O. Curnick, T. Reisch, P. Adcock, K. Ronaszegi, J.B. Robinson, D.J.L. Brett, Dead-ended anode polymer electrolyte fuel cell stack operation investigated using electrochemical impedance spectroscopy, off-gas analysis and thermal imaging, *J. Power Sources* 254 (2014) 1–9.
- J.O. Jensen, D. Aili, Y. Hu, L.N. Cleemann, Q. Li, High-temperature polymer electrolyte membrane fuel cells, in: N. Nakashima (Ed.), *Nanocarbons for Energy Conversion: Supramolecular Approaches*, Springer, Cham, 2019, pp. 45–79.
- J.O. Jensen, H.A. Hjuler, D. Aili, Q. Li, Introduction, in: Q. Li (Ed.), *High Temperature Polymer Electrolyte Membrane Fuel Cells*, Springer International Publishing Switzerland, 2016.
- C. Spiegel, Phosphoric acid fuel cells (PAFCs), in: K.P. McCoombs, L. Hagar (Eds.), *Designing and Building Fuel Cells*, McGraw-Hill, 2007.
- K. Mitsuda, T. Murahashi, Air and fuel starvation of phosphoric acid fuel cells: a study using a single cell with multi-reference electrodes, *J. Appl. Electrochem.* 21 (1991) 524–530.
- G. Li, P.G. Pickup, Measurement of single electrode potentials and impedances in hydrogen and direct methanol PEM fuel cells, *Electrochim. Acta* 49 (2004) 4119–4126.
- S. Kaserer, C. Rakousky, J. Melke, C. Roth, Design of a reference electrode for high-temperature PEM fuel cells, *J. Appl. Electrochem.* 43 (2013) 1069–1078.
- H. Kuhn, B. Andreas, A. Wokaun, G.G. Scherer, Electrochemical impedance spectroscopy applied to polymer electrolyte fuel cells with a pseudo reference electrode arrangement, *Electrochim. Acta* 51 (2006) 1622–1628.

- [38] J.L. Jespersen, E. Schaltz, S.K. Kær, Electrochemical characterization of a polybenzimidazole-based high temperature proton exchange membrane unit cell, *J. Power Sources* 191 (2009) 289–296.
- [39] F. Mack, R. Laukenmann, S. Galbiati, J.A. Keres, R. Zeis, Electrochemical impedance spectroscopy as a diagnostic tool for high-temperature PEM fuel cells, *ECS Trans.* 69 (2015) 1075–1087.
- [40] M. Mamlouk, K. Scott, Analysis of high temperature polymer electrolyte membrane fuel cell electrodes using electrochemical impedance spectroscopy, *Electrochim. Acta* 56 (2011) 5493–5512.
- [41] S.M.R. Niya, M. Hoorfar, Study of proton exchange membrane fuel cells using electrochemical impedance spectroscopy technique - a review, *J. Power Sources* 240 (2013) 281–293.
- [42] T.E. Springer, T.A. Zawodzinski, M.S. Wilson, S. Gottesfeld, Characterization of polymer electrolyte fuel cells using AC impedance spectroscopy, *J. Electrochem. Soc.* 143 (1996) 587–599.
- [43] X. Yuan, H. Wang, J.C. Sun, J. Zhang, AC impedance technique in PEM fuel cell diagnosis - a review, *Int. J. Hydrogen Energy* 32 (2007) 4365–4380.
- [44] S. Latorrata, R. Pelosato, P.G. Stampino, C. Cristiani, G. Dotelli, Use of electrochemical impedance spectroscopy for the evaluation of performance of PEM fuel cells based on carbon cloth gas diffusion electrodes, *J. Spectrosc.* (2018) 1–13, 2018.
- [45] N. Wagner, Characterization of membrane electrode assemblies in polymer electrolyte fuel cells using a.c. impedance spectroscopy, *J. Appl. Electrochem.* 32 (2002) 859–863.
- [46] E. Engebretsen, G. Hinds, Q. Meyer, T. Mason, E. Brightman, L. Castanheira, P. R. Shearing, D.J.L. Brett, Localised electrochemical impedance measurements of a polymer electrolyte fuel cell using a reference electrode array to give cathode specific measurements and examine membrane hydration dynamics, *J. Power Sources* 382 (2018) 38–44.
- [47] M. Heinzmann, A. Weber, E. Ivers-Tiffée, Impedance modelling of porous electrode structures in polymer electrolyte membrane fuel cells, *J. Power Sources* 444 (2019) 227279.
- [48] B. Andreas, A.J. McEvoy, G.G. Scherer, Analysis of performance losses in polymer electrolyte fuel cells at high current densities by impedance spectroscopy, *Electrochim. Acta* 47 (2002) 2223–2229.
- [49] E. Barsoukov, J.R. Macdonald, *Impedance Spectroscopy: Theory, Experiment, and Applications*, second ed. ed., Wiley Online, 2005.
- [50] H. Schichlein, A.C. Müller, M. Voigts, A. Krügel, E. Ivers-Tiffée, Deconvolution of electrochemical impedance spectra for the identification of electrode reaction mechanisms in solid oxide fuel cells, *J. Appl. Electrochem.* 32 (2002) 875–882.
- [51] R.M. Pooss, J.G. Kirkwood, Electrical properties of solids. VIII. Dipole moments in polyvinyl chloride-diphenyl systems, *J. Am. Chem. Soc.* 63 (1941) 385–394.
- [52] E. Ivers-Tiffée, A. Weber, Evaluation of electrochemical impedance spectra by the distribution of relaxation times, *J. Ceram. Soc. Jpn.* 125 (2017) 193–201.
- [53] J. Illig, M. Ender, A. Weber, E. Ivers-Tiffée, Modeling graphite anodes with serial and transmission line models, *J. Power Sources* 282 (2015) 335–347.
- [54] J. Illig, J.P. Schmidt, M. Weiss, A. Weber, E. Ivers-Tiffée, Understanding the impedance spectrum of 18650 LiFePO₄-cells, *J. Power Sources* 239 (2013) 670–679.
- [55] A. Leonide, V. Sonn, A. Weber, E. Ivers-Tiffée, Evaluation and modeling of the cell resistance in anode-supported solid oxide fuel cells, *J. Electrochem. Soc.* 155 (2008) B36–B41.
- [56] D. Papurello, D. Menichini, A. Lanzini, Distributed relaxation times technique for the determination of fuel cell losses with an equivalent circuit model to identify physicochemical processes, *Electrochim. Acta* 258 (2017) 98–109.
- [57] J.P. Schmidt, P. Berg, M. Schönleber, A. Weber, E. Ivers-Tiffée, The distribution of relaxation times as basis for generalized time-domain models for Li-ion batteries, *J. Power Sources* 221 (2013) 70–77.
- [58] Y. Zhang, Y. Chen, M. Yan, F. Chen, Reconstruction of relaxation time distribution from linear electrochemical spectroscopy, *J. Power Sources* 283 (2015) 464–477.
- [59] F. Ciucci, C. Chen, Analysis of electrochemical impedance spectroscopy data using the distribution of relaxation times: a bayesian and hierarchical bayesian approach, *Electrochim. Acta* 167 (2015) 439–454.
- [60] T.H. Wan, M. Saccoccio, C. Chen, F. Ciucci, Influence of the discretization methods on the distribution of relaxation times deconvolution: implementing radial basis functions with DRTtools, *Electrochim. Acta* 184 (2015) 483–499.
- [61] A. Weiß, S. Schindler, S. Galbiati, M.A. Danzer, R. Zeis, Distribution of relaxation times analysis of high-temperature PEM fuel cell impedance spectra, *Electrochim. Acta* 230 (2017) 391–398.
- [62] F. Mack, M. Klages, J. Scholta, L. Jörissen, T. Morawietz, R. Hiesgen, D. Kramer, R. Zeis, Morphology studies on high-temperature polymer electrolyte membrane fuel cell electrodes, *J. Power Sources* 255 (2014) 431–438.
- [63] D.J.L. Brett, S. Atkins, N.P. Brandon, V. Vesovic, N. Vasileiadis, A. Kucernak, Localized impedance measurements along a single channel of a solid polymer fuel cell, *Electrochim. Solid State Lett.* 6 (2003) A63–A66.
- [64] D. Kramer, I.A. Schneider, A. Wokaun, G.G. Scherer, Oscillations in the gas channels - the forgotten player in impedance spectroscopy in polymer electrolyte fuel cells B. Modeling the wave, *ECS Trans.* 3 (2006) 1249–1258.
- [65] I.A. Schneider, S.A. F. D. Kramer, A. Wokaun, G.G. Scherer, Oscillations in gas channels Part I. The forgotten player in impedance spectroscopy in PEFCs, *J. Electrochem. Soc.* 154 (2007) B383–B388.
- [66] A.A. Kulikovskiy, A model for local impedance of the cathode side of PEM fuel cell with segmented electrodes, *J. Electrochem. Soc.* 159 (2012) F294–F300.
- [67] W. Maier, T. Arlt, C. Wannek, I. Manke, H. Riesemeier, P. Krüger, J. Scholta, W. Lehnert, J. Banhart, D. Scholten, In-situ synchrotron X-ray radiography on high temperature polymer electrolyte fuel cells, *Electrochem. Commun.* 12 (2010) 1436–1438.
- [68] W. Maier, T. Arlt, K. Wippermann, C. Wannek, I. Manke, W. Lehnert, D. Stolten, Correlation of synchrotron X-ray radiography and electrochemical impedance spectroscopy for the investigation of HT-PEFCs, *J. Electrochem. Soc.* 159 (2012) F389–F404.
- [69] C. Wannek, I. Konradi, J. Mergel, W. Lehnert, Redistribution of phosphoric acid in membrane electrode assemblies for high-temperature polymer electrolyte fuel cells, *Int. J. Hydrogen Energy* 34 (2009) 9479–9485.
- [70] S.H. Eberhardt, F. Marone, M. Stampanoni, F.N. Büchi, T.J. Schmidt, Operando X-ray tomographic microscopy imaging of HT-PEFC: a comparative study of phosphoric acid electrolyte migration, *J. Electrochem. Soc.* 163 (2016) F842–F847.
- [71] S.H. Eberhardt, M. Toulec, F. Marone, M. Stampanoni, F.N. Büchi, T.J. Schmidt, Dynamic operation of HT-PEFC: in-operando imaging of phosphoric acid profiles and (Re)distribution, *J. Electrochem. Soc.* 162 (2015) F310–F316.
- [72] N. Bevilacqua, M.G. George, S. Galbiati, A. Bazylak, R. Zeis, Phosphoric acid invasion in high temperature PEM fuel cell gas diffusion layers, *Electrochim. Acta* 257 (2017) 89–98.
- [73] S. Chevalier, M. Fazeli, F. Mack, S. Galbiati, I. Manke, A. Bazylak, R. Zeis, Role of the microporous layer in the redistribution of phosphoric acid in high temperature PEM fuel cell gas diffusion electrodes, *Electrochim. Acta* 212 (2016) 187–194.
- [74] Y. Oono, A. Sounai, M. Hori, Influence of the phosphoric acid-doping level in a polybenzimidazole membrane on the cell performance of high-temperature proton exchange membrane fuel cells, *J. Power Sources* 189 (2009) 943–949.
- [75] Y. Oono, A. Sounai, M. Hori, Long-term cell degradation mechanism in high-temperature proton exchange membrane fuel cells, *J. Power Sources* 210 (2012) 366–373.
- [76] S. Han, Y.H. Jeong, J.H. Jung, A. Begley, E. Choi, S.J. Yoo, J.H. Jang, H.-J. Kim, S. W. Nam, J.Y. Kim, Spectrophotometric analysis of phosphoric acid leakage in high-temperature phosphoric acid-doped polybenzimidazole membrane fuel cell application, *J. Sensors* (2016) 8, 2016.
- [77] S. Yu, L. Xiao, B.C. Benicewicz, Durability studies of PBI-based high temperature PEMFCs, *Fuel Cell* 3–4 (2008) 165–174.
- [78] W. Maier, T. Arlt, K. Wippermann, C. Wannek, I. Manke, W. Lehnert, D. Stolten, Correlation of synchrotron X-ray radiography and electrochemical impedance spectroscopy for the investigation of HT-PEMFCs, *J. Electrochem. Soc.* 159 (2012) F398–F404.
- [79] S.H. Eberhardt, T. Lochner, F.N. Büchi, T.J. Schmidt, Correlating electrolyte inventory and lifetime of HT-PEFC by accelerated stress testing, *J. Electrochem. Soc.* 162 (2015) F1367–F1372.
- [80] C. Wannek, B. Kohnen, H.F. Oetjen, H. Lippert, J. Mergel, Durability of ABPBI-based MEAs for high temperature PEMFCs at different operating conditions, *Fuel Cell* 2 (2008) 87–95.
- [81] F. Zhou, S.J. Andreasen, S.K. Kær, J.O. Park, Experimental investigation of carbon monoxide poisoning effect on a PBI/H₃PO₄ high temperature polymer electrolyte membrane fuel cell: influence of anode humidification and carbon dioxide, *Int. J. Hydrogen Energy* 40 (2015) 14932–14941.
- [82] K. Yezerska, A. Dushina, F. Liu, M. Rastedt, P. Wagner, A. Dyck, M. Wark, Characterization methodology for anode starvation in HT-PEM fuel cells, *Int. J. Hydrogen Energy* 44 (2019) 18330–18339.
- [83] B.K. Hong, P. Mandal, J.G. Oh, S. Litster, On the impact of water activity on reversal tolerant fuel cell anode performance and durability, *J. Power Sources* 328 (2016) 280–288.
- [84] A.D. Modestov, M.R. Tarasevich, V.Y. Filimonov, E.S. Davydova, CO tolerance and CO oxidation at Pt and Pt-Ru anode catalysts in fuel cell with polybenzimidazole-H₃PO₄ membrane, *Electrochim. Acta* 55 (2010) 6073–6080.
- [85] K. Yezerska, F. Liu, A. Dushina, O. Sergeev, P. Wagner, A. Dyck, M. Wark, Analysis of the regeneration behavior of high temperature polymer electrolyte membrane fuel cells after hydrogen starvation, *J. Power Sources* 449 (2020) 227562.
- [86] R. O'Hayre, S.-W. Cha, W. Colella, F.B. Prinz, *Fuel Cell Reaction Kinetics*, Fuel Cell Fundamentals, Wiley, 2016, pp. 77–116.
- [87] R. He, Q. Li, G. Xiao, N.J. Bjerrum, Proton conductivity of phosphoric acid doped polybenzimidazole and its composites with inorganic proton conductors, *J. Membr. Sci.* 226 (2003) 169–184.
- [88] F. Mack, S. Heissler, R. Laukenmann, R. Zeis, Phosphoric acid distribution and its impact on the performance of polybenzimidazole membranes, *J. Power Sources* 270 (2014) 627–633.